inorganics

MDPI

Article

Unveiling the Effect of Solution Concentration on the Optical and Supercapacitive Performance of $CoWO_4$ Nanoparticles Prepared via the Solvothermal Method

Sagar M. Mane [1], Aviraj M. Teli [2], Sonali A. Beknalkar [2], Jae Cheol Shin [2,*] and Jaewoong Lee [1,*]

[1] Department of Fiber System Engineering, Yeungnam University, 280 Dehak-Ro, Gyeongsan 38541, Republic of Korea
[2] Division of Electronics and Electrical Engineering, Dongguk University-Seoul, Seoul 04620, Republic of Korea
* Correspondence: jcshin@dgu.ac.kr (J.C.S.); jaewlee@yu.ac.kr (J.L.)

Abstract: This study explores the influence of solution concentration, specifically that of water and ethylene glycol mixtures, on the optical and supercapacitive properties of cobalt tungstate ($CoWO_4$) nanoparticles. $CoWO_4$ nanoparticles were synthesized using varying ratios of water to ethylene glycol to ascertain the optimal conditions for enhanced performance. Detailed characterization was conducted using UV–Vis spectroscopy, photoluminescence (PL) spectroscopy, cyclic voltammetry (CV), and galvanostatic charge–discharge (GCD) to evaluate the optical properties and electrochemical behavior, respectively. The results revealed that the solution concentration significantly impacted the bandgap, absorbance, and emission properties of the $CoWO_4$ nanoparticles. Effective bandgap tuning was achieved by altering the solution concentration. When using only water, the nanoparticles displayed the lowest bandgap of 2.57 eV. In contrast, a solution with equal water and ethylene glycol concentrations resulted in the highest bandgap of 2.65 eV. Additionally, the electrochemical studies demonstrated that the water/ethylene glycol ratio markedly influenced the charge storage capacity and cyclic stability of the nanoparticles. The results indicated that the solvent concentration significantly influenced the crystallinity, particle size, and surface morphology of the $CoWO_4$ nanoparticle nanoparticles, which affected their optical properties and electrochemical performance. Notably, nanoparticles synthesized with a 1.25:0.75 proportion of water to ethylene glycol exhibited superior supercapacitive performance, with a specific capacitance of 661.82 F g^{-1} at a current density of 7 mA cm^{-2} and 106% capacitance retention after 8000 charge–discharge cycles. These findings underscore the critical role of solvent composition in tailoring the functional properties of $CoWO_4$ nanoparticles, providing insights for their application in optoelectronic devices and energy storage systems.

Keywords: $CoWO_4$ nanoparticles; solvothermal synthesis; effect of solvent concentration; optical properties; supercapacitor performance

Citation: Mane, S.M.; Teli, A.M.; Beknalkar, S.A.; Shin, J.C.; Lee, J. Unveiling the Effect of Solution Concentration on the Optical and Supercapacitive Performance of $CoWO_4$ Nanoparticles Prepared via the Solvothermal Method. *Inorganics* **2024**, *12*, 203. https://doi.org/10.3390/inorganics12080203

Academic Editor: Chek Hai Lim

Received: 3 July 2024
Revised: 25 July 2024
Accepted: 26 July 2024
Published: 29 July 2024

1. Introduction

The ever-growing demand for high-performance energy storage devices and advanced optical materials has spurred intensive research into nanostructured materials, with a specific focus on improving the performance and efficiency of these technologies [1]. Supercapacitors have emerged as a crucial component in this field of energy conversion and storage applications due to their high power density, rapid charge/discharge cycles, and long-term stability. These features make supercapacitors an appealing alternative to traditional batteries, especially for applications needing quick energy bursts and extended operational lifespans [2–4]. Within the diverse array of materials investigated for supercapacitor and optoelectronic applications, materials from the metal tungstate family such as $CuWO_4$, $NiWO_4$, $FeWO_4$, $ZnWO_4$, $CoWO_4$, $CeWO_4$, and $MnWO_4$ have shown exceptional promise. This is because metal tungstates have favorable characteristics that make them

ideal for energy storage device applications, such as significant specific capacitance, high power density, high specific surface area, and great rate capability [5–8]. Furthermore, materials from the metal tungstate family have garnered significant attention in optoelectronic applications. This interest stems from their optical properties, including a wide bandgap and strong absorption in the visible region, as well as their use in scintillators. Additionally, their combination of semiconducting characteristics and nonlinear optical properties further enhances their appeal [9–13].

In the metal tungstate family, cobalt tungstate ($CoWO_4$) nanoparticles have attracted considerable interest due to their unique electrical, magnetic, and optical properties. Due to these promising features, $CoWO_4$ has gained a great deal of attention in various technological applications, which include catalysts, microwave dielectrics, wastewater treatment, nonenzymatic glucose sensing, acetone sensing, an anode for Li-ion batteries, photoluminescence, dye-sensitized solar cells (DSSCs), optical fibers, humidity sensors, optoelectronics, tribological devices, and electrocatalysis [9–14]. The distinctive advantages of $CoWO_4$ nanoparticles stem from their high theoretical capacitance, excellent conductivity, and robust structural integrity. These properties facilitate efficient electron transfer and robust energy storage capabilities, making $CoWO_4$ an ideal candidate for supercapacitors. The superior electrochemical performance of $CoWO_4$ nanoparticles can be attributed to their intrinsic characteristics, such as a large surface area, high porosity, and favorable crystalline structure. These attributes enable the nanoparticles to store a greater amount of charge and deliver it rapidly when needed [7,15]. Furthermore, this p-type semiconductor reflects enriched conductivity in the range of 10^{-7} to 10^{-3} $S.cm^{-1}$, which is higher than that of pure metal oxide counterparts. This enrichment is mainly ascribable to the incorporation of tungstate [7,15,16].

In addition to the abovementioned technological applications of $CoWO_4$, this bimetallic tungstate is also very suitable for optoelectronic applications, such as photodetectors and light-emitting devices [17]. The bandgap of $CoWO_4$ is typically in the range of 2.2 to 2.8 eV, which classifies it as a semiconductor. On the other hand, the luminescence of $CoWO_4$ is mainly due to the electronic transitions within the Co^{2+} ions. When excited by UV light, $CoWO_4$ can emit light in the visible range, which is often observed as a characteristic blue or green emission [9,13,18,19]. In general, $CoWO_4$ crystallizes in a monoclinic wolframite structure. This structure is characterized by chains of edge-sharing octahedra, where cobalt (Co) and tungsten (W) ions are coordinated by oxygen (O) atoms. This monoclinic symmetry further leads to anisotropic optical properties, and the material exhibits different optical behavior along different crystallographic directions [18–20]. However, the functional properties of $CoWO_4$ nanoparticles are significantly influenced by the choice of synthesis methods, temperature, time variation, and solvents used during their preparation. The solvothermal method, a widely used synthesis technique, enables precise control over the morphology and size of nanoparticles, while solvents such as water and ethylene glycol play a crucial role in determining the morphology, size, and distribution of the nanoparticles [16]. A few studies have revealed that the physiochemical properties of the nanoparticles can be tuned with the use of alternative solvents in the preparation of nanoparticles [2,7,12,16]. Furthermore, the concentration of these solvents affects the crystallinity and surface chemistry of $CoWO_4$, thereby impacting its optical and supercapacitive performance. However, there are no studies in the literature that examine how changes in solvent concentrations affect the physicochemical properties of the materials, specifically for metal tungstate-based nanoparticles such as $CoWO_4$ nanoparticles. Therefore, understanding the influence of solution concentration on the properties of $CoWO_4$ nanoparticles holds substantial significance for both fundamental science and practical applications. From a scientific perspective, it provides insights into the nucleation and growth mechanisms of nanoparticles in varying chemical environments, contributing to the broader knowledge base regarding nanomaterial synthesis. Practically, optimizing the concentration can lead to the development of $CoWO_4$-based materials with tailored proper-

ties for specific applications, such as more efficient supercapacitors for energy storage and enhanced optical devices.

This research focuses on the synthesis of $CoWO_4$ nanoparticles using the solvothermal method, with a particular emphasis on understanding how the concentration of the precursor solution affects their optical and supercapacitive properties. The primary objectives of this research are to synthesize and characterize $CoWO_4$ nanoparticles with varying precursor concentrations; systematically investigate their optical properties; and evaluate their electrochemical performance as supercapacitor electrodes, focusing on specific capacitance and cycling stability as a function of solution concentration. By systematically analyzing how the mixed-solvent environment affects the structural and functional properties of $CoWO_4$, this research seeks to uncover the optimal conditions for maximizing their performance. The addition of ethylene glycol during the preparation of $CoWO_4$ nanoparticles enhances their electrochemical performance. An electrode made of nanoparticles prepared with a solvent volume ratio of 1.25:0.75 (water/ethylene glycol) has the highest specific capacitance, while all the electrodes have over 100% stability after 8000 charge–discharge cycles measured at 25 mA cm^{-2}. Furthermore, the bandgap of the $CoWO_4$ nanoparticles can easily tuned by changing the solvent proportion; the estimated bandgap remains between 2.57 to 2.65 eV for the different ratios of water to ethylene glycol. These insights related to electrochemical and optical properties presented through this work will not only advance the fundamental understanding of $CoWO_4$ nanoparticle synthesis but also contribute to the development of high-performance materials for energy storage and optoelectronic applications.

2. Results and Discussion

Using X-ray diffraction (XRD), the produced materials' phase purity and structural characterization were ascertained. Even without any additional heat treatment or annealing process, all samples of $CoWO_4$ had strong, sharp diffraction peaks, confirming formation with good crystallinity, as illustrated in Figure 1a. The observed crystal plane positions closely match the monoclinic crystal symmetry with space group P2/c of $CoWO_4$, as referenced by JCPDF number 01-072-0479 [3]. The monoclinic crystallinity remains the same during the preparation of $CoWO_4$ nanoparticles with the involvement of ethylene glycol in the total solvent. The impact on various parameters, including plane position, peak intensity, and average crystallite size of the nanoparticles, was significant. Figure 1b confirms this, showing a magnified view of the system's most intense crystal plane at $2\theta = 30.6^{\circ}$. With the addition of ethylene glycol at an initial ratio of 1.75:0.25, the crystal plane positions shifted towards a lower 2θ angle. As the ratio of ethylene glycol in the solvent increased, the peak position started to move towards a higher 2θ angle. When the concentration of ethylene glycol became equal to that of DI water, the peak position slightly shifted back towards a lower 2θ angle. Furthermore, as the ethylene glycol content increased, the intensity of the crystal peaks decreased. The average crystallite size of each $CoWO_4$ sample was estimated by analyzing six highly intense crystal planes from each diffraction pattern, specifically (100), (110), (−111), (002), (−202), and (−132). The Debye–Scherrer equation was applied to estimate the average crystallite size as illustrated below [9].

$$D = \frac{k\lambda}{\beta cos\theta} \quad (1)$$

This equation relates the crystallite size (D) to the broadening (peak width) of the crystal plane, centered at a specific angle (θ) and measured at half the maximum height, known as FWHM or β. In the equation, λ represents the X-ray wavelength, and k is the shape factor constant. A decrease in average crystallite size was observed with an increasing ratio of ethylene glycol in the solvent mixture, except at a 1:1 ratio, where the size increased. All samples indicated the formation of nanosized crystallites, with estimated sizes ranging from 15 to 25 nm. The estimated lattice parameters, unit cell volume, and

crystallite size for samples prepared with different ratios of DI water to ethylene glycol are summarized in Table 1.

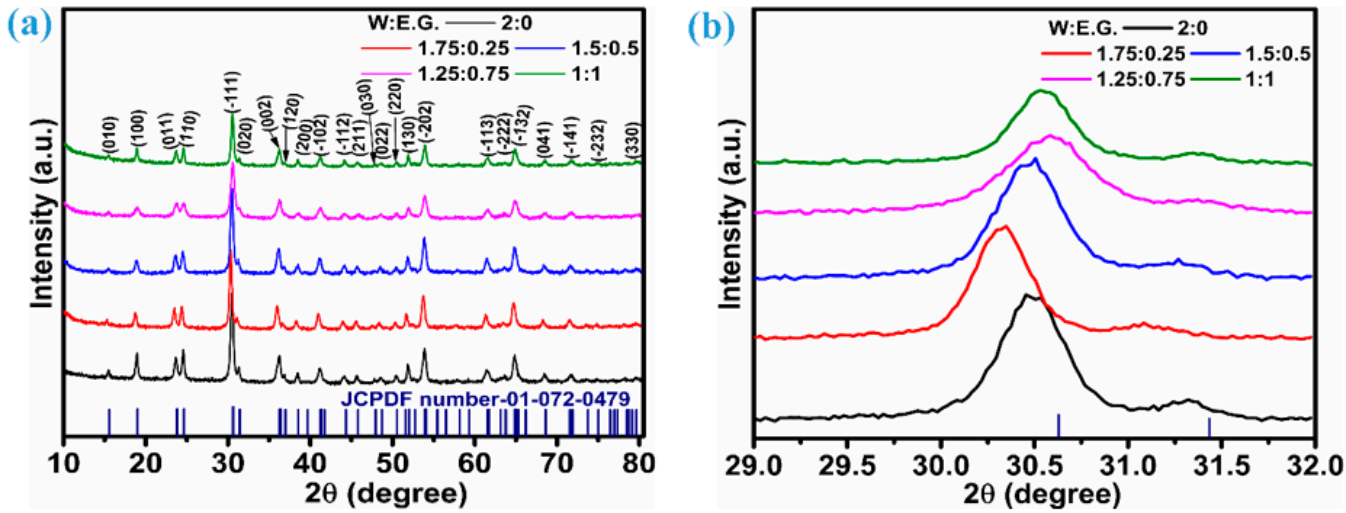

Figure 1. (**a**) X-ray diffraction patterns of the $CoWO_4$ nanoparticles at different solvent concentrations; (**b**) magnified view of the (−111) crystal plane for all samples.

Table 1. Various parameters estimated from the analysis of the X-ray diffraction patterns of the $CoWO_4$ nanoparticles prepared with different solvent ratios.

W/E.G. Ratio	Lattice Parameters (Å)			Angles (θ)			Volume (V)	Crystallite Size (nm)
	a	b	c	α	β	γ		
2:0	4.646	5.694	4.959	90	90.228	90	131.31	22.71
1.75:0.25	4.646	5.695	4.959	90	90.282	90	131.21	21.68
1.5:0.5	4.646	5.699	4.959	90	90.247	90	131.20	19.31
1.25:0.75	4.646	5.692	4.958	90	90.354	90	131.15	15.99
1:1	4.646	5.693	4.959	90	90.275	90	131.16	24.46

The functional characteristics and chemical bond information of all $CoWO_4$ samples were determined using Fourier transform infrared (FTIR) spectroscopy analysis, as depicted in Figure 2. Figure 2 is divided into two sections: one covering the range from 1750 to 400 cm^{-1} and the other ranging from 4000 to 2750 cm^{-1}. The section between 2750 and 1750 cm^{-1}, which contains no absorption bands, has been omitted to emphasize the regions with absorption bands. The absorption bands that are visible within the 400–1000 cm^{-1} wavenumber range are associated with the $CoWO_4$ nanoparticles' stretching vibrations. The bands within this range of wavenumbers are the primary bands resulting from the absorption of the wolframite-type structure in metal tungstates [21]. The vibration at 827 cm^{-1} signifies the anti-symmetric stretching involving the O-W-O bonds [9,13], while the bands at 621 cm^{-1} and 951 cm^{-1} are associated with the stretching vibrations of the W-O bonds [22]. The absorptions observed at 459 cm^{-1} and 510 cm^{-1} correspond to the symmetrical and asymmetrical deformations of the W-O and Co-O bonds within the WO_6 and CoO_6 polyhedra, respectively [21,23]. Absorption at 1383 cm^{-1} indicates the symmetrical stretching of the C=O bond, attributed to the presence of a hydroxyl functional group [24]. The depth of this band seems to be enhanced with increasing content of ethylene glycol. The subsequent spectral absorption peak at 1629 cm^{-1} indicates stretching involving either C=N or H-O-H bending [10,21,25]. Symmetric stretching of the C-H bond is attributable to the absorptions at 2886 cm^{-1} and 2977 cm^{-1} [11], while the broad absorption centered around 3407 cm^{-1} corresponds to the stretching vibrations indicative

of water (OH) molecules adsorbed on the powder's surface. These vibrations are linked to the presence of moisture during the test preparation [22,25].

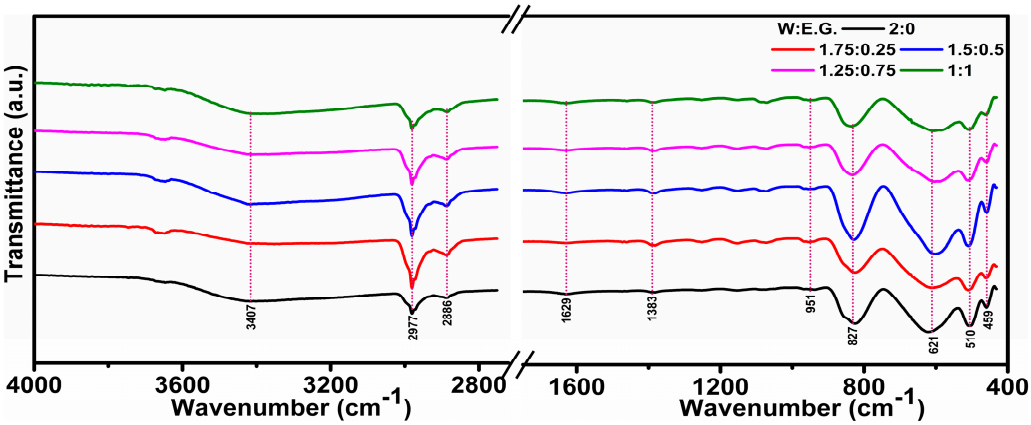

Figure 2. FT-IR spectra of $CoWO_4$ nanoparticles at different solvent concentrations.

X-ray photoelectron spectroscopy (XPS) was applied to probe the surface atomic composition and binding energies in cobalt tungstate nanoparticles synthesized with a solvent ratio of 1.25:0.75. Surface scanning, as illustrated in Figure 3a, captured only the spectra related to the constituent elements, i.e., Co, W, and O, respectively, without peaks of any other element. The deconvoluted Co 2p spectrum as represented in Figure 3b provides detailed insights into the contributions from different chemical states or environments of cobalt atoms in a sample. Two strong asymmetric peaks at 780.2 eV and 796.5 eV were visible in the Co 2p spectra, signifying the two states Co $2p_{3/2}$ and Co $2p_{1/2}$, respectively. Inside these asymmetric reflections, the Co^{3+} species of cobalt atom was identified as the source of the peaks at 780.0 eV and 796.1 eV. On the other hand, the Co^{2+} states of this element were centered at 781.3 eV and 797.1 eV [6,8,26]. Two further subpeaks were linked to satellite levels, which were centered at 785.3 eV and 803.1 eV. The presence of satellite levels with reasonable intensity signifies the existence of a Co^{2+} oxidation state in the Co 2p spectrum of the Co element [27]. The W4f spectrum featured two distinct peaks at 34.9 eV and 37.0 eV, corresponding to the characteristic reflections of the element W. These peaks indicated the presence of W $4f_{7/2}$ and W $4f_{5/2}$, respectively. The fitted spectrum for the element W had a spin–orbit separation of 2.1 eV, as shown in Figure 3c, confirming its existence in the 6^+ oxidation state [8,27,28]. Due to metal–oxygen bonds, the O 1s spectrum split into two main peaks at 529.8 eV (corresponding to Co–O and W–O bonds) and 530.6 eV, as displayed in Figure 3d [2,27]. The atomic percentages of Co, W, and O determined from XPS were 15.1%, 16.3%, and 68.6%, respectively, indicating the formation of $CoWO_4$.

Figure 4a–j displays the FE-SEM images of $CoWO_4$ nanoparticles at various magnifications, prepared using different ratios of ethylene glycol in the total solvent. Specifically, Figures (a and b), (c and d), (e and f), (g and h), and (i and j) show the surface microstructure images of samples prepared with 2:0, 1.75:0.25, 1.5:0.5, 1.25:0.75, and 1:1 ratios of deionized water to ethylene glycol, respectively. These images revealed that all microstructures appeared identical, confirming the formation of clustered granule-like nanoparticles, indicating that $CoWO_4$ forms without structural modification despite variations in ethylene glycol content. However, changes in particle size were observed with the addition of ethylene glycol. Histograms of the particle size, derived using ImageJ (Version-1.54 j) software with log-normal plots, are shown in Figure 4k–o. These histograms indicate that the sample prepared with a 1:1 solvent ratio had a higher number of larger particles (approximately 47 nm) than the other samples. Samples prepared with 1.5:0.5 and 1.25:0.75 ratios had the highest number of particles below 30 nm, while samples with only water and a 1.75:0.25 ratio had the majority of their particles around 35 nm in size. These observations were also recorded in the X-ray diffraction analysis. The $CoWO_4$ nanoparticles

(synthesized with a 1.25:0.75 ratio of water to ethylene glycol) underwent EDS analysis to assess their elemental composition and purity. Figure S1 (Supporting Information) presents the EDS spectrum, displaying energy peaks corresponding to Co, W, and O elements. The estimated atomic percentages of these elements are shown in the accompanying table, which aligns closely with the observations from the XPS results.

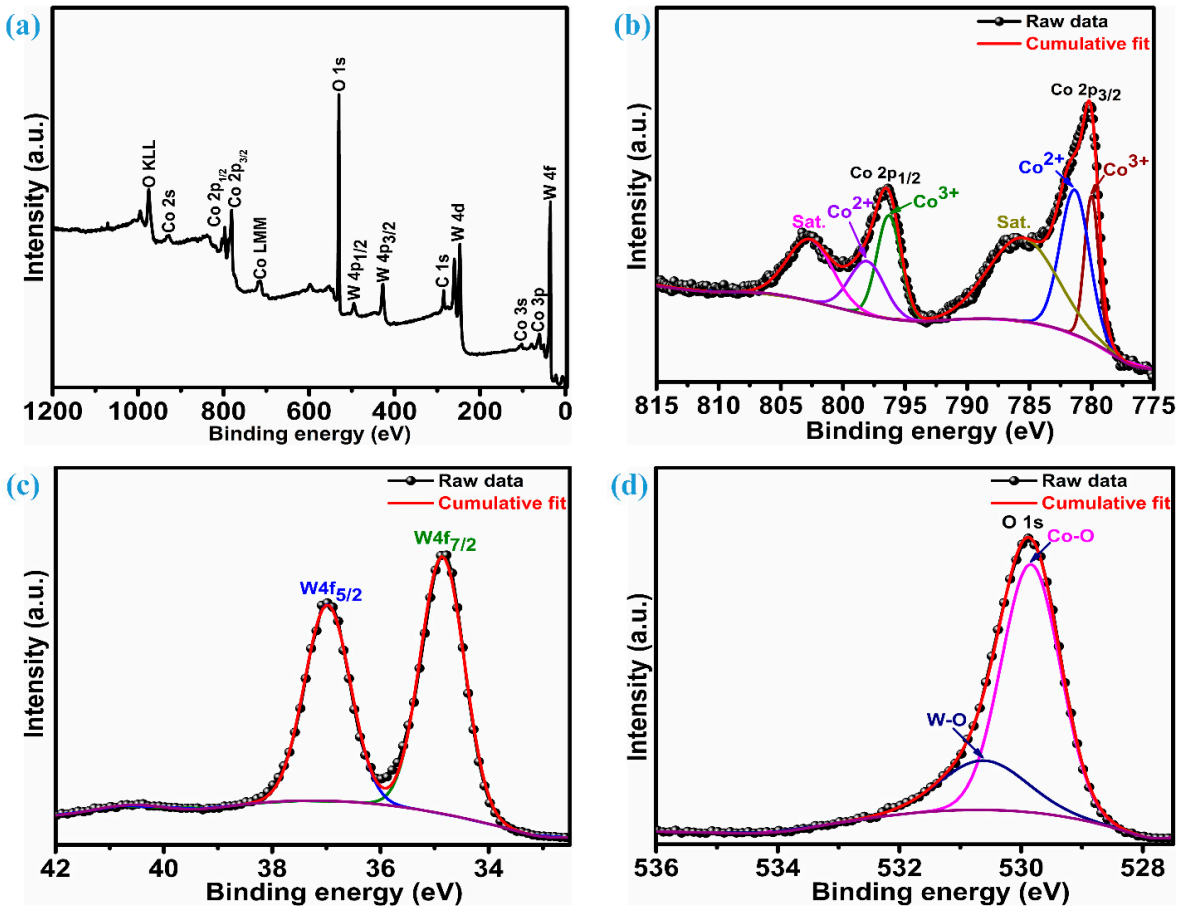

Figure 3. XPS analysis of the $CoWO_4$ nanoparticles prepared with a 1.25:0.75 ratio of water to ethylene glycol: (**a**) survey spectrum, (**b**) high-resolution spectrum of Co 2p, (**c**) high-resolution spectrum of W 4f, and (**d**) high-resolution spectrum of O 1s.

Brunauer–Emmett–Teller (BET) analysis is a critical characterization technique that provides valuable insights into the surface properties of $CoWO_4$ nanoparticles synthesized via the solvothermal method. Surface area is a crucial factor in determining the activity and efficiency of nanoparticles in various applications. In this context, all samples of $CoWO_4$ nanoparticles were subjected to BET analysis to elucidate how changes in solution concentration translate to variations in surface area and pore structure. The N_2 adsorption–desorption curves, depicted in Figure 5a–e for various solvent concentrations, exhibited a characteristic Type IV isotherm, indicative of the mesoporous nature of the $CoWO_4$ nanoparticles. For supercapacitive applications, a higher BET surface area often indicates a higher number of active sites accessible for electrochemical processes [1]. Comparably, a more expansive surface area with larger active sites is also helpful in improving a nanoparticle's optical characteristics by enhancing its contact with light [29]. Specifically, $CoWO_4$ nanoparticles prepared with a 1:0.75 ratio of water to ethylene glycol exhibited a higher surface area of 33.76 m^2g^{-1}. As confirmed by BET analysis, other samples of $CoWO_4$ nanoparticles exhibited a surface area of 15.09, 16.93, 20.52, and 26.10 m^2g^{-1} for water/ethylene glycol ratios of 2:0, 1.75:0.25, 1.5:0.5, and 1:1 respectively. The BET surface area significantly impacts the optical properties and supercapacitive performance

of $CoWO_4$ nanoparticles. A larger surface area enhances light absorption, beneficial for photocatalysis and photodetectors, and correlates with increased capacitance in supercapacitors by providing more active sites for electrochemical reactions [16,29,30]. Mesoporous structures with an optimal pore size facilitate electrolyte diffusion and ionic transport, which are essential for high-rate supercapacitor performance. Additionally, these pores can trap and scatter light, influencing the optical behavior of the nanoparticles. The pore size distribution of the $CoWO_4$ nanoparticles was analyzed using the BJH method. Figure 5f–j illustrate the pore size distribution for $CoWO_4$ nanoparticles at various water/ethylene glycol concentrations. The estimated pore volumes were 0.1459, 0.1479, 0.1261, 0.1699, and 0.1357 cm^3g^{-1} for the nanoparticle samples with water/ethylene glycol ratios of 2:0, 1.75:0.25, 1.5:0.5, 1.25:0.75, and 1:1, respectively. The pore structure from BET analysis is crucial, as mesoporous materials exhibit unique optical behaviors by interacting with light. Equally important, mesopores facilitate rapid ion transport, essential for high power density and cyclic stability in supercapacitors [1,29].

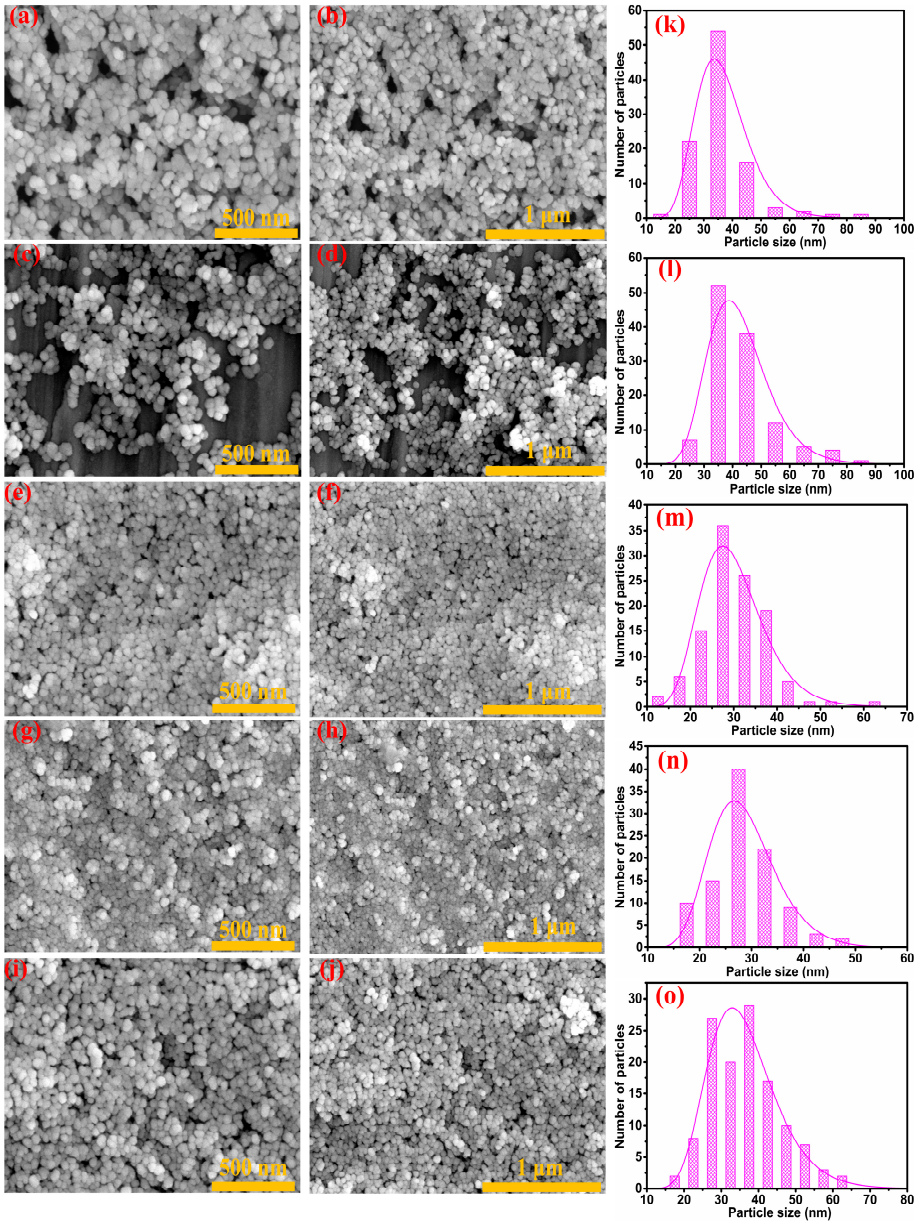

Figure 4. Morphology (FE-SEM) and particle-size analysis of the $CoWO_4$ nanoparticles prepared with different solvent concentrations: (**a**,**b**)—2:0, (**c**,**d**)—1.75:0.25, (**e**,**f**)—1.5:0.5, (**g**,**h**)—1.25:0.75, (**i**,**j**)—1:1; (**k**–**o**) particle-size analysis using image j-software for respective $CoWO_4$ nanoparticles.

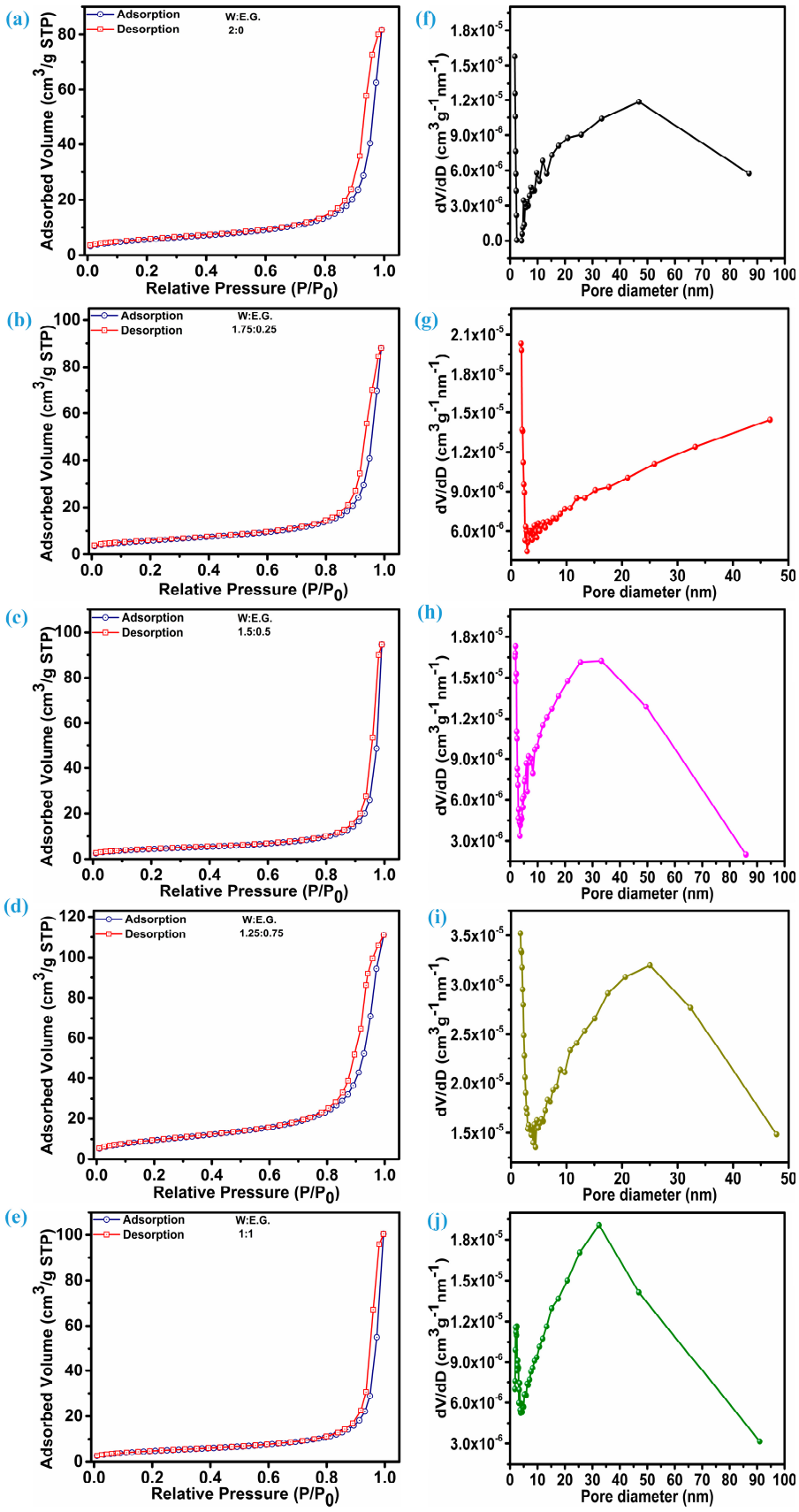

Figure 5. BET analysis. (**a**–**e**) N_2 adsorption–desorption isotherms and (**f**–**j**) pore size distribution based on the BJH method for $CoWO_4$ nanoparticles prepared with different solvent concentrations.

Figure 6a shows the diffuse reflectance absorption spectra for $CoWO_4$ nanoparticles. These spectra exhibited an absorption band ranging from 350 nm to 800 nm for all the samples prepared in this study. Each sample displayed a broad absorption peak centered at 586 nm, accompanied by a smaller shoulder peak at 523 nm. The d-d transitions between the $^4A_2 \rightarrow {}^4T_{1(P)}$ energy levels of Co^{2+} ions are responsible for this broad absorption peak [11]. Another absorption noted below 450 nm is characteristic of electron excitation from the O_{2p} orbital of the oxygen element towards the W_{5d} orbital of the tungsten element, resulting from UV energy absorption [10,13]. Close observation revealed that the absorption edge initially decreased with the addition of ethylene glycol. It then increased sharply for the samples prepared with solvent ratios of 1.5:0.5 and 1.25:0.75. Finally, when the solvent was in equal proportion, the absorption edge decreased again, indicating an increase in the bandgap. The Tauc plot of each sample is illustrated in Figure 6b, which was further utilized to estimate the binding energy as per the equation below [12].

$$(\alpha h\upsilon) = A(h\upsilon - E_g)^2 \quad (2)$$

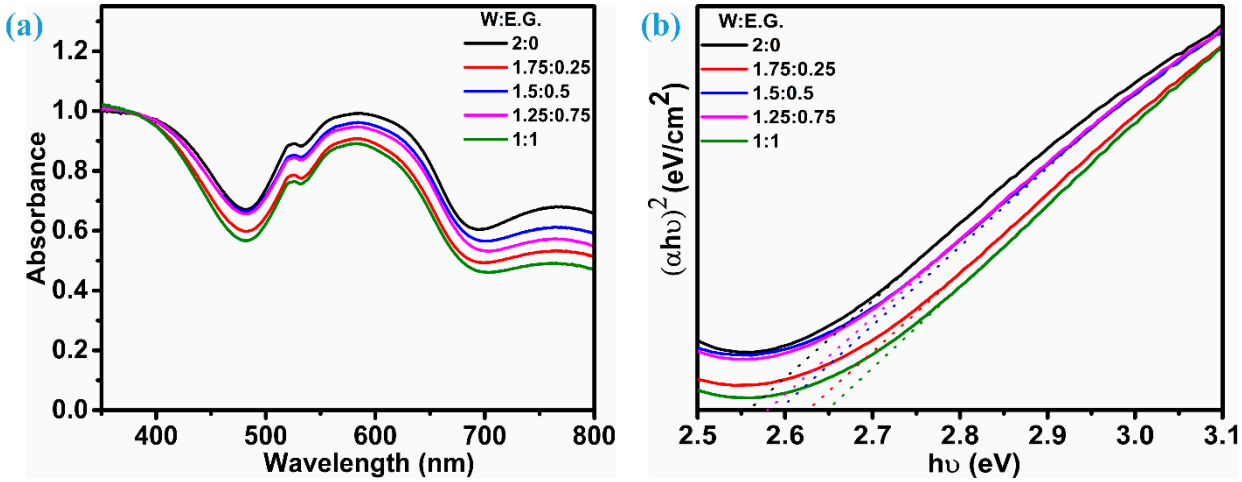

Figure 6. UV–Vis spectra. (**a**) Absorbance spectra for all samples of $CoWO_4$ nanoparticles and (**b**) estimation of bandgap.

In this equation, α denotes the absorption coefficient, A is a constant, and h and v are Planck's constant and the radiation frequency, respectively. The estimated bandgap values lie in the range of 2.57 to 2.65 eV. Bandgap tuning was observed as the solvent ratio changed: E_g increased with the initial addition of ethylene glycol, then decreased again. For samples with solvent concentrations of 1.5:0.5 and 1.25:0.75, E_g remained almost the same. However, when the ethylene glycol concentration increased and became equal in proportion, the bandgap increased again. This increase may be attributed to the variation in particle size and other several factors including the complex interplay of variables, solvent interactions, change in synthesis conditions concerning variation in the solvent ratio, quantum confinement effects, defects, and states of aggregation and dispersion. Additionally, orbital overlapping plays a significant role in changes in the bandgap: a reduction in overlapping reduces the bandgap, and vice versa [13,31].

Figure 7 illustrates the photoluminescence characteristics of $CoWO_4$ nanoparticles synthesized with varying water/ethylene glycol ratios measured at a 520 nm excitation wavelength. Usually, the energy produced during the recombination of photogenerated carriers leads to the emission of photoluminescence (PL). The intensity of the characteristic PL peak indicates the recombination rate in the material. A lower PL intensity signifies a lower recombination rate, while a higher intensity indicates a higher recombination rate. Materials with lower recombination rates, and thus lower PL intensities, are particularly useful for catalytic applications [14]. A strong, broad spectrum centered at 470 nm for each sample of $CoWO_4$ nanoparticles indicates blue-green emission. The shoulder peaks visible

on either side of this broad spectrum are signatures of radiative transitions within the $[WO_4]^{2-}$ tetrahedral group [17]. Notably, the broad spectrum exhibited the lowest intensity when $CoWO_4$ nanoparticles were prepared using a solvent ratio of 1.25:0.75. Consequently, this sample demonstrates higher electrocatalytic activity than the others.

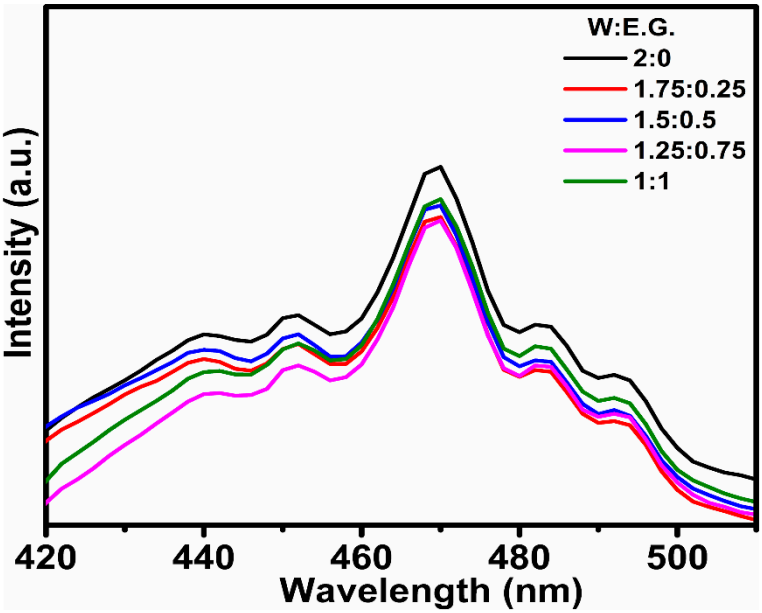

Figure 7. Photoluminescence spectrum for all samples of CoWO4 nanoparticles.

Measurements of the electrochemical performance of $CoWO_4$ nanoparticle electrodes made at different solution concentrations were carried out in an aqueous KOH electrolyte. The purpose of this study was to determine how small variations in solution concentration impact the supercapacitive capabilities of $CoWO_4$ nanoparticles. Figure 8a illustrates cyclic voltammetry curves that compare electrodes made from $CoWO_4$ nanoparticles prepared with different concentrations of solvent solutions. These measurements were taken at a scan rate of 20 mV s^{-1} within a potential range of −0.2 to 0.6 V. The results indicate that the $CoWO_4$ nanoparticles prepared with a water/ethylene glycol ratio of 1.25:0.75 exhibited the largest area under the curve, suggesting optimal performance at this concentration. The shape of the CV itself had a different nature than observed for electrochemical double-layer capacitors, with the distinct presence of redox peaks implying that all samples of $CoWO_4$ nanoparticles exhibit pseudocapacitive behavior [3,6,7]. This was further analyzed by measuring the CV profiles of each electrode at varying scan rates from 5 mV s^{-1} to 100 mV s^{-1} as illustrated in Figure 8b–f. The tungsten does not participate in this redox reaction; instead, it significantly enhances the overall conductivity. Therefore, these redox peaks on both the reduction and oxidation sides stem from the reversible electrochemical reaction between Co^{2+} and Co^{3+} species. This is a clear indication that the faradic mechanism predominantly governs the overall charge storage process [8,32,33]. Each of these electrodes persisted in outstanding reversibility as indicated by the symmetry redox peaks. Peak current climbed as the scan rate and accompanying peak potential in both cases moved slightly outward, while no change was noticed in the overall shape. Effectively, this conduction is a very important factor for the effective movement of ions and electrons between the electrode and the electrolyte at their interface [6,8]. This process was more pronounced for $CoWO_4$ nanoparticles prepared with a solvent ratio of 1.25:0.75, as this electrode could achieve a higher current level than nanoparticles prepared with other solvent ratios.

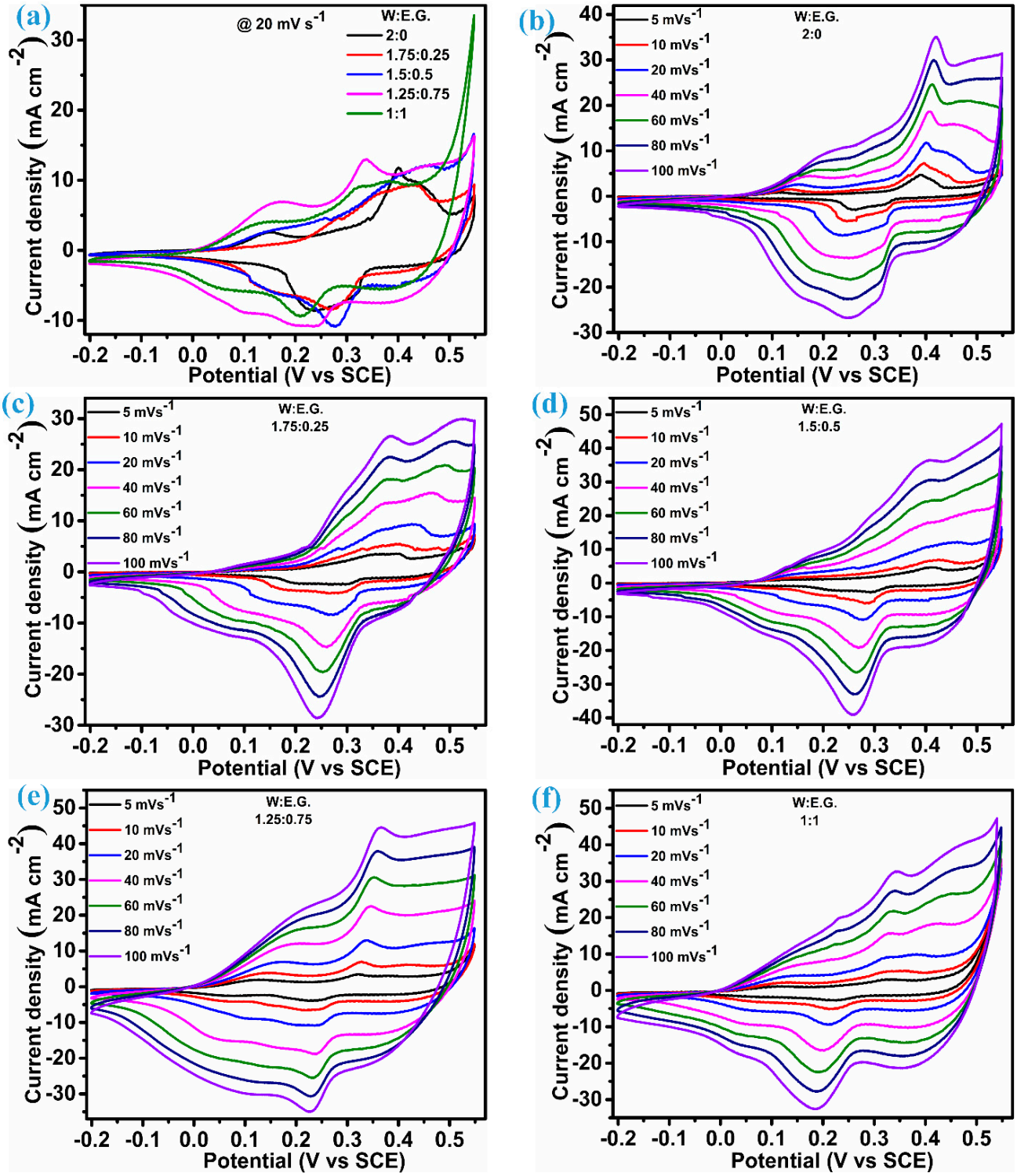

Figure 8. Cyclic voltammetry curves (**a**) for all electrodes of $CoWO_4$ nanoparticles at 20 mV s^{-1}, (**b**) at various scan rates for $CoWO_4$ nanoparticles prepared with a solvent ratio of 2:0, (**c**) at various scan rates for $CoWO_4$ nanoparticles prepared with a solvent ratio of 1.75:0.25, (**d**) at various scan rates for $CoWO_4$ nanoparticles prepared with a solvent ratio of 1.5:0.5, (**e**) at various scan rates for $CoWO_4$ nanoparticles prepared with a solvent ratio of 1.25:0.75, and (**f**) at various scan rates for $CoWO_4$ nanoparticles prepared with a solvent ratio of 1:1.

Constant-current charge–discharge measurements were been employed to further examine the electrode with optimal performance. Figure 9a presents a comparative analysis

of the charge–discharge curves for all electrodes at 7 mA cm^{-2}. All electrodes had a well-defined plateau during discharge, which is an indication of their pseudocapacitive nature [7,34]. Moreover, GCD confirmed that the $CoWO_4$ nanoparticles prepared with a solvent ratio of 1.25:0.75 exhibited optimal specific capacitance compared to other electrodes, as it reflected higher discharge time; this was also evidenced by the CV analysis. According to equations 1 and 2, the estimation of specific capacitance (areal capacitance) revealed that the highest value of 661.82 F g^{-1} (1985.4 mF cm^{-2}) at 7 mA cm^{-2} was achieved when the nanoparticles were prepared with a water/ethylene glycol ratio of 1.25:0.75. The values of specific capacitance (areal capacitance) for $CoWO_4$ nanoparticles prepared with ratios of 2:0, 1.75:0.25, 1.5:0.5, and 1:1 were 358.1 F g^{-1} (930.86 mF cm^{-2}), 386.4 F g^{-1} (966 mF cm^{-2}), 516.55 F g^{-1} (1498 mF cm^{-2}), and 498.75 F g^{-1} (1396.5 mF cm^{-2}), respectively. Further GCD measurements were carried out at up to twice the original current density, i.e., 14 mA cm^{-2} for each electrode. These curves are represented in Figure 9b–f, suggesting a decline in capacitance with increasing current density. The delay in fast faradic redox reactions results in the active material not reacting promptly; hence, the specific capacitance declines at higher current densities [34]. Values of specific capacitance estimated at various current densities are shown in Figure 9g. The highest retention, 86.29%, was observed for $CoWO_4$ nanoparticles prepared with a solvent ratio of 1.5:0.5 at 14 mA cm^{-2}, compared to the value at 7 mA cm^{-2}, as depicted in Figure 9h. All electrodes demonstrate excellent retention ability, maintaining over 75% retention when the current density is doubled which is an indication high stability of the $CoWO_4$ nanoparticles.

To evaluate the cycling performance of each $CoWO_4$ electrode, charge–discharge measurements were conducted up to 8000 cycles at a current density of 25 mA cm^{-2}. Figure 10a–e are composed of the charge–discharge performance and related coulombic efficiency over 8000 cycles for the $CoWO_4$ nanoparticles prepared with 2:0, 1.75:0.25, 1.5:0.5, 1.25:0.75, and 1:1 ratios of water to ethylene glycol, respectively. The electrode containing nanoparticles made at a solvent ratio of 1.75:0.25 exhibited superior stability compared to the others. It retained 168% of its original capacitance after 8000 cycles. Each electrode showed distinct cycling performance. The electrode with the best performance (solvent ratio 1.25:0.75) demonstrated an initial increase in capacitance up to 2000 cycles, stabilizing thereafter. For electrodes prepared with $CoWO_4$ nanoparticles and solvent ratios of 2:0, 1.5:0.5, and 1:1, there was an initial increase in capacitance, which then decreased with more cycles. However, the most stable electrode exhibited a sustained increase in capacitance throughout the cycling process. This continuous growth in capacitance (stability) for electrodes with $CoWO_4$ nanoparticles made at solvent ratios of 1.75:0.25 and 1.25:0.75 is mainly due to the formation of numerous diffusion channels and the larger surface area of the electrode, enhancing interaction with the electrolyte [35]. The coulombic efficiency of each electrode was slightly below 100% for the first few cycles. It then rose to just above 100% and remained stable, except for the electrodes prepared with 2:0 and 1.5:0.5 solvent ratios. These electrodes showed slight fluctuations, with minor increases and decreases, throughout the cycling process. These observations of coulombic efficiency indicate that electron trapping across the solid-electrolyte interphase layer was minimal, allowing more electrons to participate in reversible electrochemical reactions [36]. To confirm stability exceeding 100% after 8000 cycles, charge–discharge measurements were conducted at a current density of 7 mA cm^{-2}. These results were then compared with the initial charge–discharge curve obtained before cycling, under the same current density. These results are illustrated in the inset figures of the stability curves for each electrode of the $CoWO_4$ nanoparticles.

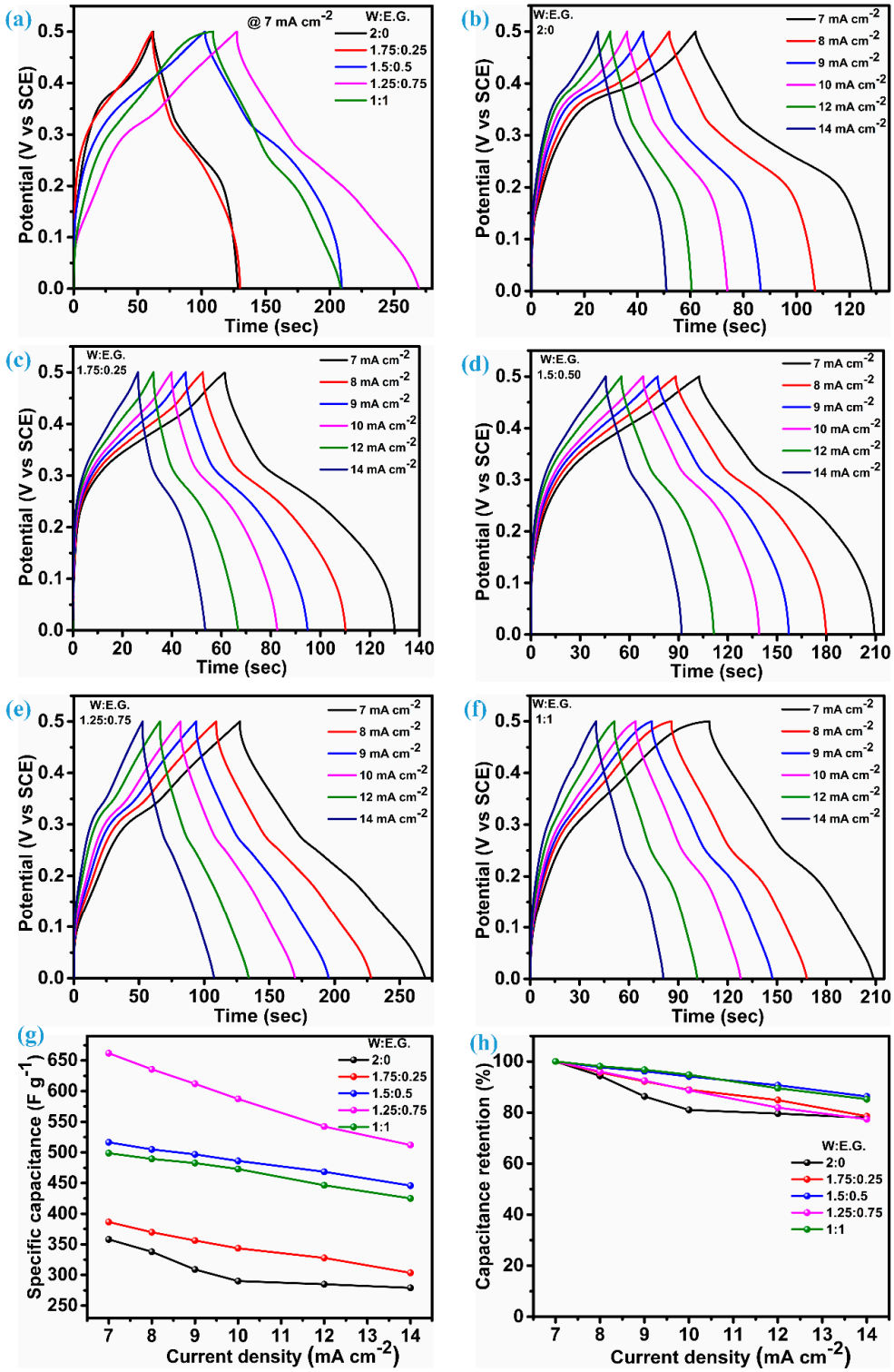

Figure 9. Charge–discharge profiles and estimation of capacitance. (**a**) GCD for all electrodes of $CoWO_4$ nanoparticles at 7 mA cm^{-2}, (**b**) GCD at various current densities for $CoWO_4$ nanoparticles prepared with a solvent ratio of 2:0, (**c**) GCD at various current densities for $CoWO_4$ nanoparticles prepared with a solvent ratio of 1.75:0.25, (**d**) GCD at various current densities for $CoWO_4$ nanoparticles prepared with a solvent ratio of 1.5:0.5, (**e**) GCD at various current densities for $CoWO_4$ nanoparticles prepared with a solvent ratio of 1.25:0.75, (**f**) GCD at various current densities for $CoWO_4$ nanoparticles prepared with a solvent ratio of 1:1, (**g**) specific capacitance at different current density of all electrodes, and (**h**) capacitance retention at various current density.

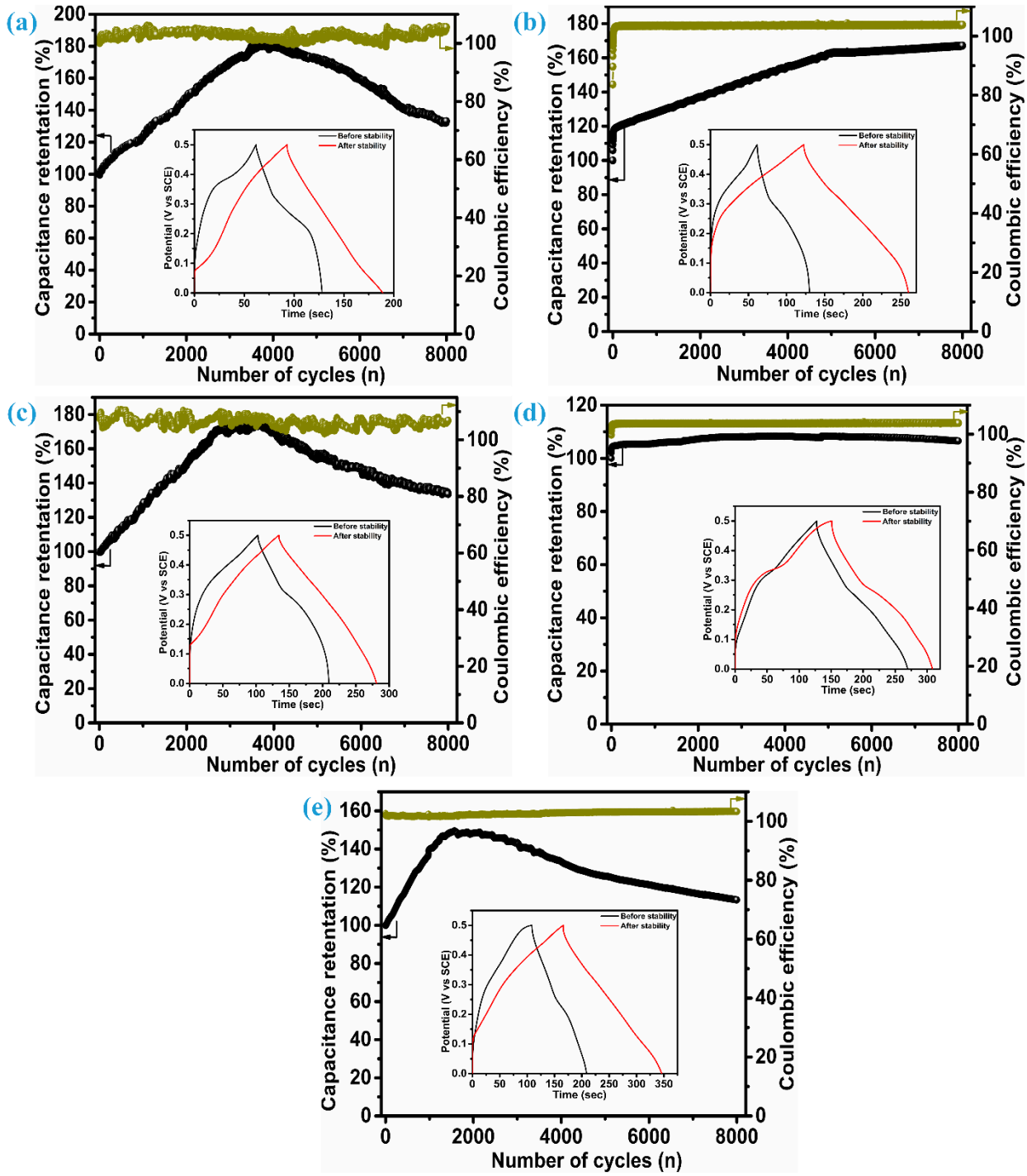

Figure 10. Cyclic stability and coulombic efficiency up to 8000 cycles (**a**) for the electrode of $CoWO_4$ nanoparticles prepared with a solvent ratio of 2:0, (**b**) for the electrode of $CoWO_4$ nanoparticles prepared with a solvent ratio of 1.75:0.25, (**c**) for the electrode of $CoWO_4$ nanoparticles prepared with a solvent ratio of 1.5:0.5, (**d**) for the electrode of $CoWO_4$ nanoparticles prepared with a solvent ratio of 1.25:0.75, and (**e**) for the electrode of $CoWO_4$ nanoparticles prepared with a solvent ratio of 1:1 (GCD profiles inset are before and after stability for respective electrode).

Electrochemical impedance spectroscopy (EIS) measurements, as shown in Figure 11a for all electrodes of the $CoWO_4$ nanoparticles, revealed a bifurcation of these curves in both the high-frequency and low-frequency regions. In the high-frequency region, the spectra indicate the series resistance (Rs), which is identified by the point of intersection

with the real (x) axis. The second region, corresponding to the low-frequency range, indicates the charge transfer resistance. Typically, this is represented by the diameter of the semicircle observed in this region [34]. The electrodes made from $CoWO_4$ nanoparticles prepared with water/ethylene glycol ratios of 1.5:0.5 and 1.25:0.75 exhibited the lowest series resistance, measuring 0.39 Ω cm^{-2}. The magnified view of the Nyquist plot, shown in Figure 11b, provides additional confirmation. Moreover, the electrode with the optimal specific capacitance exhibited the lowest charge-transfer resistance of 0.5 Ω cm^{-2}, which was the lowest among all tested electrodes. These values indicate that this electrode material established excellent contact with the current collector (Ni foam), outperforming others in this regard. Furthermore, a more pronounced straight-line trend along the y-axis in the EIS plot for this electrode suggests higher ion mobility, contributing to its elevated specific capacitance among other electrodes made of $CoWO_4$ nanoparticles.

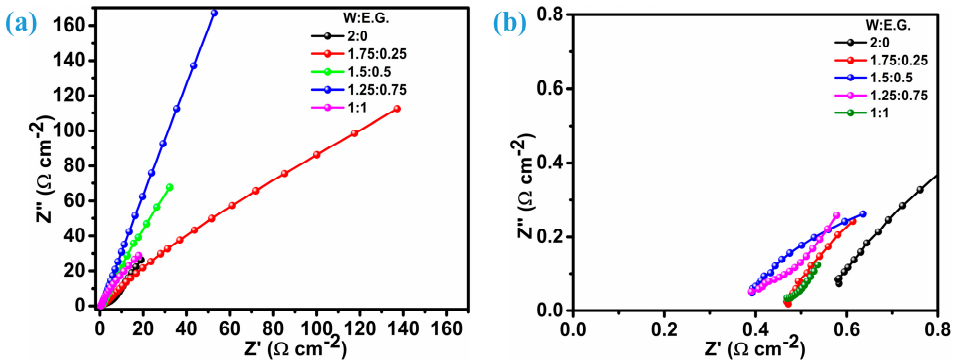

Figure 11. (**a**) EIS spectrum for all samples of $CoWO_4$ nanoparticles. (**b**) A magnified view of the EIS spectrum at the intersection of the x-axis.

3. Experimental Details

3.1. Materials

Precursors including cobalt (II) chloride hexahydrate ($CoCl_2 \cdot 6H_2O$), sodium tungstate dihydrate ($Na_2WO_4 \cdot 2H_2O$), and ethylene glycol were obtained from Sigma Aldrich (St. Louis, MO, USA).

3.2. Synthesis of $CoWO_4$ Nanoparticles

$CoWO_4$ nanoparticles were synthesized using a solvothermal synthesis approach where the ratio of water to ethylene glycol was systematically varied. In simple steps of synthesis, 50 mM of $CoCl_2 \cdot 6H_2O$ was first added to 80 mL (DI water) of solvent in a beaker, and continuous stirring was applied for up to 15 min. Following this step, the same amount of $Na_2WO_4 \cdot 2H_2O$ in a 1:1 proportion was added directly to the solution containing $CoCl_2 \cdot 6H_2O$, and continuous stirring was further provided for 30 min to ensure homogeneity. The homogeneous solution containing cobalt and tungstate precursors was poured into a 125 mL Teflon liner. The Teflon liner was then sealed inside a stainless steel autoclave and maintained at 180 °C for 24 h. After the reaction was complete and the autoclave had cooled to room temperature, the $CoWO_4$ nanoparticles were collected. The collected nanoparticles were washed with water and ethanol to remove any residual solvents and by-products and dried at 100 °C for 24 h. This process was repeated, gradually replacing the volume of water with ethylene glycol, until a 1:1 volume ratio of deionized water to ethylene glycol was achieved. The dried $CoWO_4$ nanoparticles were used for further characterization, as well as electrochemical and optical measurements, without any additional annealing or heating processes.

3.3. Characterization Techniques

X-ray diffraction (XRD) was performed using a DIATOME-Pananlytical instrument (Malvern, UK) with Cu Kα radiation (1.54 Å). X-ray photoelectron spectroscopy (XPS) anal-

ysis was conducted using a Versaprobe II system (ULVAC-PHI Inc., Chigasaki, Kanagawa, Japan). Field-emission scanning electron microscopy (FE-SEM) was carried out using an S-4800 microscope (Hitachi, Ibaraki, Japan). Functional characteristics were analyzed using Fourier transform infrared (FT-IR) spectra (PerkinElmer FT-IR spectrometer- Spectrum 100, Waltham, MA, USA). Optical features (absorbance range and bandgap energy) were determined using ultraviolet–visible (UV–Vis) diffuse reflectance measurements (Agilent Technologies, Cary 5000 UV–Vis spectrometer, Santa Clara, CA, USA). The properties of photoluminescence were evaluated using a fluorescence spectrometer with a xenon source (Hitachi, F-7000, Tokyo, Japan).

3.4. Electrode Fabrication and Electrochemical Measurements

The $CoWO_4$ nanoparticles in powdered form obtained after drying were used to fabricate the electrodes on Ni foam. To fabricate the electrode, powdered nanoparticles were mixed with PVDF and carbon black in N-methyl-2-pyrrolidinone, maintaining a ratio of 80:10:10. Before applying slurries of this mixture to coat a 1 cm^2 area of Ni foam, the foam was thoroughly cleaned using ultrasonic treatment with ethanol, acetone, and deionized water. Following the application of the mixed slurries, the Ni foam was dried at 80 °C overnight and utilized further for analyzing electrochemical features. All measurements were carried out with a three-electrode system in which 2 mol/L potassium hydroxide (KOH) was used as an electrolyte. An electrochemical workstation ZIVE SP5 (WonaTech, Seocho-gu, Seoul, Republic of Korea) was used to conduct all the electrochemical assessments. The electrochemical performance of each electrode was evaluated in terms of specific capacitance (using weight of active material deposited) and areal capacitance (using active area immersed in the electrolyte) using the following equations [37]:

$$C_s = \frac{I \times t_d}{m \times \Delta V} \tag{3}$$

$$C_s = \frac{I \times t_d}{A \times \Delta V} \tag{4}$$

In the first expression, 'm' represents the weight of the active material, 'I' is the current density, 't_d' is the discharge time, and 'ΔV' is the voltage window. The active-material weights for the electrode are 2.6, 2.5, 2.9, 3.0, and 2.8 mg cm^{-2} for $CoWO_4$ nanoparticles prepared with DI water and glycol in ratios of 2:0, 1.75:0.25, 1.5:0.5, 1.25:0.75, and 1:1, respectively. Similarly, 'A' in the second expression represents the active area of the electrode.

4. Conclusions

This investigation into the effects of solution concentration (ethylene glycol/water) on the optical and supercapacitive performance of $CoWO_4$ nanoparticles concluded with noteworthy discoveries. Changes in the solvent content by even a very small fraction were discovered to affect the optical properties, such as bandgap energy and absorption characteristics. The optical properties can be effectively tuned by adjusting the solvent ratio during nanoparticle preparation, suggesting promising applications in optoelectronic devices. Furthermore, different concentrations impacted the $CoWO_4$ nanoparticles' specific capacitance and charge–discharge cycling stability in supercapacitive performance, highlighting the significance of solvent selection in maximizing electrochemical characteristics. This study implies the possible usefulness of more research into variables such as temperature and pH, which may make it easier to create multifunctional nanomaterials such as $CoWO_4$. These initiatives may open the door to a variety of technical uses for such materials.

Supplementary Materials: The following supporting information can be downloaded at: https://www.mdpi.com/article/10.3390/inorganics12080203/s1, Figure S1: EDS spectra of the $CoWO_4$ nanoparticles prepared with a 1.25:0.75 ratio of water-to-ethylene glycol.

Author Contributions: Conceptualization, S.M.M.; methodology, S.M.M.; software, S.M.M.; validation, A.M.T., J.C.S. and J.L.; formal analysis, S.A.B.; investigation, S.M.M.; resources, A.M.T. and S.A.B.; data curation, S.M.M.; writing—original draft preparation, S.M.M.; writing—review and editing, S.M.M. and J.L.; visualization, J.C.S.; supervision, J.L.; project administration, J.L.; funding acquisition, J.L. All authors have read and agreed to the published version of the manuscript.

Funding: This work was supported by a Korea Institute for Advancement of Technology (KIAT) grant funded by the Korean Government (Ministry of Trade, Industry, and Energy—MOTIE), grant number (P0012770).

Data Availability Statement: Dataset available on request from the authors.

Conflicts of Interest: The authors declare no conflicts of interest.

References

1. Askari, M.B.; Jamali, F.; Tourchi Moghadam, M.T.; Azizi, S.; Seifi, M. Synthesis and Characterization of $MnWO_4$-CNT for Supercapacitor Applications. *Sustainability* **2023**, *15*, 14910. [CrossRef]
2. Patil, S.S.; Chougale, U.M.; Kambale, R.K.; Fulari, V.J. Hydrothermal Synthesis of $CoWO_4$ Nanoparticles and Evaluation of Their Supercapacitive Performance. *J. Energy Storage* **2023**, *67*, 107517. [CrossRef]
3. Patil, S.J.; Chodankar, N.R.; Huh, Y.S.; Han, Y.K.; Lee, D.W. Bottom-up Approach for Designing Cobalt Tungstate Nanospheres through Sulfur Amendment for High-Performance Hybrid Supercapacitors. *ChemSusChem* **2021**, *14*, 1602–1611. [CrossRef] [PubMed]
4. Sardar, K.; Thakur, S.; Maiti, S.; Besra, N.; Bairi, P.; Chanda, K.; Majumdar, G.; Chattopadhyay, K.K. Amalgamation of $MnWO_4$ nanorods with Amorphous Carbon Nanotubes for Highly Stabilized Energy Efficient Supercapacitor Electrodes. *Dalton Trans.* **2021**, *50*, 5327–5341. [CrossRef] [PubMed]
5. He, G.; Li, J.; Li, W.; Li, B.; Noor, N.; Xu, K.; Hu, J.; Parkin, I.P. One Pot Synthesis of Nickel Foam Supported Self-Assembly of $NiWO_4$ and $CoWO_4$ Nanostructures That Act as High Performance Electrochemical Capacitor Electrodes. *J. Mater. Chem. A Mater.* **2015**, *3*, 14272–14278. [CrossRef]
6. Zhang, M.; Fan, H.; Zhao, N.; Peng, H.; Ren, X.; Wang, W.; Li, H.; Chen, G.; Zhu, Y.; Jiang, X.; et al. 3D Hierarchical $CoWO_4/Co_3O_4$ Nanowire Arrays for Asymmetric Supercapacitors with High Energy Density. *Chem. Eng. J.* **2018**, *347*, 291–300. [CrossRef]
7. Xing, X.; Gui, Y.; Zhang, G.; Song, C. $CoWO_4$ Nanoparticles Prepared by Two Methods Displaying Different Structures and Supercapacitive Performances. *Electrochim. Acta* **2015**, *157*, 15–22. [CrossRef]
8. Rajkumar, S.; Christy Ezhilarasi, J.; Saranya, P.; Princy Merlin, J. Fabrication of $CoWO_4$/PANI Composite as Electrode Material for Energy Storage Applications. *J. Phys. Chem. Solids* **2022**, *162*, 110500. [CrossRef]
9. Oliveira, Y.L.; Gouveia, A.F.; Costa, M.J.S.; Lopes, F.H.P.; Sczancoski, J.C.; Longo, E.; Luz, G.E.; Santos, R.S.; Cavalcante, L.S. Investigation of Electronic Structure, Morphological Features, Optical, Colorimetric, and Supercapacitor Electrode Properties of $CoWO_4$ Crystals. *Mater. Sci. Energy Technol.* **2022**, *5*, 125–144. [CrossRef]
10. Gao, Q.; Sun, G.; Ling, R.; Cai, Y.; Wang, A. Construction and Characterization of $CoWO_4$/g-C_3N_4 Composites for Efficient Sonocatalytic Degradation of Rhodamine B. *J. Mater. Sci. Mater. Electron.* **2022**, *33*, 25589–25602. [CrossRef]
11. Geetha, G.V.; Sivakumar, R.; Kuroki, Y.; Gopalakrishnan, C.; Sanjeeviraja, C. Structural and Optical Properties of $CoWO_4$ Nanoparticles Synthesized by Co-Precipitation Technique. In *AIP Conference Proceedings*; American Institute of Physics Inc.: College Park, MD, USA, 5 November 2020; Volume 2265.
12. Alharthi, F.A.; Al-Nafaei, W.S.; Alshayiqi, A.A.; Alanazi, H.S.; Hasan, I. Hydrothermal Synthesis of Bimetallic (Zn, Co) Co-Doped Tungstate Nanocomposite with Direct Z-Scheme for Enhanced Photodegradation of Xylenol Orange. *Catalysts* **2023**, *13*, 404. [CrossRef]
13. Jeyakanthan, M.; Subramanian, U.; Tangsali, R.B. Enhanced Photoluminescence of $CoWO_4$ in $CoWO_4/PbWO_4$ Nanocomposites. *J. Mater. Sci. Mater. Electron.* **2018**, *29*, 1914–1924. [CrossRef]
14. Nithya, P.; Roumana, C.; Velraj, G.; Balasubramanian, V.; Shkir, M.; Reddy, V.R.M. Biomass-Derived Carbon (BC) Modified $CoWO_4$ Nanoparticles Composites for Improved Performance of Dye-Sensitized Solar Cells. *Chem. Phys. Lett.* **2022**, *803*, 139814. [CrossRef]
15. Lokhande, V.; Lee, S.J.; Lokhande, A.; Kim, J.H.; Ji, T. 1.5 V Symmetric Supercapacitor Device Based on Hydrothermally Synthesized Carbon Nanotubes and Cobalt Tungstate Nanocomposite Electrodes. *Mater. Chem. Phys.* **2018**, *211*, 214–224. [CrossRef]
16. Li, A.; Tu, Y.; Zhu, Y.; Li, D.; Zhou, W.; Zhu, X.; Feng, L. $CoWO_4$ Nanoparticles Prepared in Different Solvents and Their Pseudocapacitant Performances. *Int. J. Electrochem. Sci.* **2017**, *12*, 5646–5656. [CrossRef]
17. Juliet Josephine Joy, J.; Victor Jaya, N. Structural, Magnetic and Optical Behavior of Pristine and Yb Doped $CoWO_4$ Nanostructure. *J. Mater. Sci. Mater. Electron.* **2013**, *24*, 1788–1795. [CrossRef]
18. Paul Chowdhury, A.; Shambharkar, B.H. Synthesis and Photocatalytic Properties of Sunlight-Responsive BiOBr–$CoWO_4$ Heterostructured Nanocomposites. *Appl. Organomet. Chem.* **2020**, *34*, e5436. [CrossRef]

19. Moreira, R.L.; Almeida, R.M.; Siqueira, K.P.F.; Abreu, C.G.; Dias, A. Optical Phonon Modes and Infrared Dielectric Properties of Monoclinic $CoWO_4$ Microcrystals. *J. Phys. D Appl. Phys.* **2015**, *49*, 045305. [CrossRef]
20. Ahmadi, F.; Rahimi-Nasrabadi, M.; Fosooni, A.; Daneshmand, M. Synthesis and Application of $CoWO_4$ Nanoparticles for Degradation of Methyl Orange. *J. Mater. Sci. Mater. Electron.* **2016**, *27*, 9514–9519. [CrossRef]
21. Prabakaran, P.; Prabhu, S.; Selvaraj, M.; Navaneethan, M.; Ramu, P.; Ramesh, R. Synthesis of R-GO-Incorporated $CoWO_4$ Nanostructure for High-Performance Supercapattery Applications. *J. Mater. Sci. Mater. Electron.* **2022**, *33*, 9312–9323. [CrossRef]
22. Rani, B.J.; Ravi, G.; Ravichandran, S.; Ganesh, V.; Ameen, F.; Al-Sabri, A.; Yuvakkumar, R. Electrochemically Active XWO_4 (X = Co, Cu, Mn, Zn) Nanostructure for Water Splitting Applications. *Appl. Nanosci.* **2018**, *8*, 1241–1258. [CrossRef]
23. Xing, X.; Wang, J. Reduced Graphene Oxide Incorporated $NiWO_4$ for High-Performance Energy Storage. *J. Mater. Sci. Mater. Electron.* **2016**, *27*, 11613–11622. [CrossRef]
24. Nivedha, K.; Subramanian, B. Synergistic Integration of Bi_2O_3 | |$CoWO_4$ for Asymmetric Supercapattery: A Binder-Free Approach Ensuring High Endurance Cycling Stability. *J. Energy Storage* **2023**, *72*, 109269. [CrossRef]
25. Andrade Neto, N.F.; Oliveira, Y.G.; Nascimento, J.H.O.; Bomio, M.R.D.; Motta, F.V. Influence of pH Variation on $CuWO_4$, $CuWO_4/WO_3$ and $CuWO_4/CuO$ Structures Stabilization: Study of the Photocatalytic Properties under Sunlight. *J. Mater. Sci. Mater. Electron.* **2020**, *31*, 18221–18233. [CrossRef]
26. Nasser, R.; Zhou, H.; Li, F.; Elhouichet, H.; Song, J.M. Heterostructured MoO_3@$CoWO_4$ Nanobelts towards High Electrochemical Performances via Oxygen Vacancies Generation. *J. Colloid Interface Sci.* **2024**, *654*, 805–818. [CrossRef] [PubMed]
27. Bagwade, P.P.; Magdum, V.V.; Malavekar, D.B.; Chitare, Y.M.; Gunjakar, J.L.; Patil, U.M.; Lokhande, C.D. Synthesis, Characterization and Visible Light Driven Dye Degradation Performance of One-Pot Synthesized Amorphous $CoWO_4$ Powder. *J. Mater. Sci. Mater. Electron.* **2022**, *33*, 24646–24662. [CrossRef]
28. Nasser, R.; Wang, X.L.; Tiantian, J.; Elhouichet, H.; Song, J.M. Hydrothermal Design of $CoMoO_4$@$CoWO_4$ Core-Shell Heterostructure for Flexible All-Solid-State Asymmetric Supercapacitors. *J. Energy Storage* **2022**, *51*, 104349. [CrossRef]
29. Alkallas, F.H.; Trabelsi, A.B.G.; Alrebdi, T.A.; Ahmed, A.M.; Rabia, M. Development of a Highly Efficient Optoelectronic Device Based on $CuFeO_2/CuO/Cu$ Composite Nanomaterials. *Materials* **2022**, *15*, 6857. [CrossRef]
30. Rajput, R.B.; Kale, R.B. The Facile Synthesis of 3D Hierarchical Flower-like TiO_2 Microspheres with Enhanced Photocatalytic Activity. *J. Phys. Chem. Solids* **2023**, *177*, 111286. [CrossRef]
31. Su, Y.; Zhu, B.; Guan, K.; Gao, S.; Lv, L.; Du, C.; Peng, L.; Hou, L.; Wang, X. Particle Size and Structural Control of $ZnWO_4$ Nanocrystals via Sn^{2+} Doping for Tunable Optical and Visible Photocatalytic Properties. *J. Phys. Chem. C* **2012**, *116*, 18508–18517. [CrossRef]
32. Xu, X.; Gao, J.; Huang, G.; Qiu, H.; Wang, Z.; Wu, J.; Pan, Z.; Xing, F. Fabrication of $CoWO_4$@$NiWO_4$ Nanocomposites with Good Supercapacitve Performances. *Electrochim. Acta* **2015**, *174*, 837–845. [CrossRef]
33. Xu, X.; Shen, J.; Li, N.; Ye, M. Facile Synthesis of Reduced Graphene Oxide/$CoWO_4$ Nanocomposites with Enhanced Electrochemical Performances for Supercapacitors. *Electrochim. Acta* **2014**, *150*, 23–34. [CrossRef]
34. Ge, J.; Wu, J.; Dong, J.; Jia, J.; Ye, B.; Jiang, S.; Zeng, J.; Bao, Q. Hydrothermal Synthesis of Hybrid Rod-Like Hollow $CoWO_4/Co_{1-x}S$ for High-Performance Supercapacitors. *ChemElectroChem* **2018**, *5*, 1047–1055. [CrossRef]
35. Patil, S.S.; Mane, S.M.; Nimbalkar, N.A.; Khilare, C.J.; Kulkarni, S.B.; Dhasade, S.S.; Kamat, R.K.; Lee, J.; Chavan, S.G. A Simple Facile Synthesis for Phase Transforming of δ-MnO_2 into α-MnO_2 and Thereby Enhancing Na-Ion Supercapacitive Performance. *Ionics* **2024**, *30*, 3055–3068. [CrossRef]
36. Xiao, J.; Li, Q.; Bi, Y.; Cai, M.; Dunn, B.; Glossmann, T.; Liu, J.; Osaka, T.; Sugiura, R.; Wu, B.; et al. Understanding and Applying Coulombic Efficiency in Lithium Metal Batteries. *Nat. Energy* **2020**, *5*, 561–568. [CrossRef]
37. Mane, S.M.; Teli, A.M.; Beknalkar, S.A.; Patil, D.R.; Shin, J.C.; Lee, J. Cationic-surfactant (CTAB) Assisted Preparation of 2D Graphitic Carbon Nitride (g-C_3N_4) Sheets Advances Supercapacitive Performance. *Crystals* **2024**, *14*, 312. [CrossRef]